Robotics and Computer Integrated Manufacturing 57 (2019) 477–487

Contents lists available at ScienceDirect

Robotics and Computer Integrated Manufacturing

journal homepage: www.elsevier.com/locate/rcim

Full length Article

In-process virtual verification of weld seam removal in robotic abrasive belt grinding process using deep learning

Vigneashwara Pandiyan[a], Pushparaja Murugan[a], Tegoeh Tjahjowidodo[a,*], Wahyu Caesarendra[b,c], Omey Mohan Manyar[b], David Jin Hong Then[b]

[a] School of Mechanical and Aerospace Engineering, Nanyang Technological University, Singapore 639798, Singapore
[b] Rolls-Royce@NTU Corporate Lab, Nanyang Technological University, Singapore 637460, Singapore
[c] Faculty of Integrated Technologies, Universiti Brunei Darussalam, Jalan Tungku Link, Gadong BE1410, Brunei Darussalam

ARTICLE INFO

Keywords:
Abrasive belt grinding
Deep learning
Weld seam removal
Segmentation
Vision sensor

ABSTRACT

Transforming the manufacturing environment from manually operated production units to unsupervised robotic machining centres requires a presence of reliable in-process monitoring system. In this paper, we demonstrate a technique for automatic endpoint detection of weld seam removal in a robotic abrasive belt grinding process with the help of a vision system using deep learning. The paper presents the results of the first investigative stage of semantic segmentation of weld seam removal states using encoder-decoder convolutional neural networks (EDCNN). An experimental investigation using four different weld seam states on mild steel work coupon are trained using the VGG-16 network based on encoder-decoder architecture. The results demonstrate the potential of the developed vision based methodology as a tool for endpoint prediction of the weld seam removal in real time during a compliant abrasive belt grinding process. The prediction system based on semantic segmentation is able to monitor weld profile geometry evolution taking into account the varying belt grinding parameters during machining which will allow further process optimisation.

1. Introduction

Unsupervised robotic machining centres have transformed the manufacturing environment significantly. There is a significant demand for optimal unsupervised machining centres for process monitoring [1]. Modern industries strive to develop a well optimised process to save time and money as well as to ensure the quality of the end products. Welding processes are inevitable in aerospace industries for producing complex components such as turbine blades [2,3]. However, weld seams introduced from the production cycle need to be removed to maintain the final surface within the specified tolerance. Use of abrasive belt grinding for weld seam and machining mark removal and to secure the final surface quality is a common industrial practice [4–6]. In addition, some cases of intelligent computer-vision assisted application in robotic grinding can also be found in literature [7,8]. It is accepted by the workforce as a tertiary finishing process which does not require any extra work before and after [9].

Recently, in many industrial applications, belt grinding processes are assisted by robots for surface finishing task. However, the current practice for weld seam removal still depends on an operator to manually perform the process. This brings a few concerns with regards to the consistency on the process quality as the process is highly dependent to the operator expertise, besides the workplace safety issues for the operators. In addition, manual belt grinding is also time consumptive as the components have to be transported from automated production lines to the manual machining station and vice versa. For ensuring a complete industrialised time-intensive weld seam removal work, it is vital to construct a forecasting system that can oversee the weld seam removal in real time.

The recent development in artificial intelligence is a promising exercise to improve the efficiency of automatic weld seam removal in a robotic environment. Some existing commercial automated tracked weld shaving system are available. But those require extra time for assembling and disassembling. Furthermore, these systems are specifically customised for individual components which adds to the production cost [10]. Whitney et al. [11] developed a light vision system that measures material volume removed from on weld bead during multi-pass grinding in real time. The authors have previously developed a system for real-time endpoint detection of weld seam removal on a robotic abrasive belt grinding process using discrete wavelet transform (DWT) and support vector machine (SVM) [5]. Although the methodology of using force and vibration sensor is able to estimate the weld

* Corresponding author.
E-mail address: ttegoeh@ntu.edu.sg (T. Tjahjowidodo).

https://doi.org/10.1016/j.rcim.2019.01.006
Received 10 August 2018; Received in revised form 27 December 2018; Accepted 9 January 2019
Available online 17 January 2019

seam states and to predict removed material using the machine learning classifiers, it suffers from the constraint that force and accelerometer signal change significantly based on grinding parameters. As a result, using the same classifier model for different grinding conditions will affect the performance of the prediction. In manufacturing industries, especially in surface finishing processes, weld seam occurs in complicated geometries, material and even locations that are hard to access which makes the model vulnerable as sensor signatures change drastically based on machining conditions. A more robust method has to be developed to take into account different parameters that will cater for a wider range of problems. In this paper, a methodology is proposed to determine the end point of weld seam removal process based on computer vision and deep learning that is independent to the parameters of the grinding process.

The sensitivity of the prediction depends on the selection of the sensors and their location [12,13]. Therefore, the sensors selected to be integrated into the operation is a significant factor in the overall design of the decision-making system [14,15]. Vision sensors have been extensively used in the initial weld point sensing, thus providing weld seam information for welding robot assistance [16,17]. Industrial robots that are equipped with camera have been used to monitor surface machining [18]. An intensified CCD camera setup has been developed to determine the temperature field in the cutting zone, during an orthogonal high speed machining operation [19]. LeCun et al. [20] stated that state-of-the-art developments in several technology domains such as self-driving cars [21,22], trend prediction [23,24], image recognition [25] and many other domains are made possible because of deep neural networks (DNN's). Manufacturing industries have started to adopt deep learning technique as they have shown outstanding performance and reliable results on object detection and recognition which are beneficial to automation, optimization, and cost-cutting. Gokberk et al. [26] proposed a deep learning predictive model for determining three crucial metrics of machining namely quality, performance, and energy consumption on the data generated from a 5-axis machine tool. The prediction output indicates that deep learning model offers accurate predictions and can be used in the real-time decision-making process for manufacturing industries. Encoder-decoder or SegNet architectures using DNN's produce pixel level annotations for semantic mapping are capable of detection, classification, and localization which can also be applied to solve a variety of real-world problems [27]. A reliable in-process monitoring system independent of the grinding parameter, which is developed from a vision system and encoder-decoder based deep learning architecture in this research, is also essential in realising Industry 4.0.

The paper is organized as follows: a brief outline of the industrial requirement and the research gaps in belt grinding automation is discussed in Section 1, followed by a brief theoretical basis on the belt grinding process, VGG-16 architecture and SegNet in Section 2. The grinding conditions, belt grinding setup, vision system, weld seam states are presented in Section 3. The training parameters, network learning and segmentation results discussed in Section 4. Finally, the findings of this paper and future works for further optimisation are evaluated in Section 5.

2. Theoretical basis

2.1. Abrasive belt grinding

An abrasive belt grinding process is a variation of the long-established grinding processes, where the tool is made up of the coated abrasive belt and rotating polymer contact wheel assembly as shown in Fig. 1. The polymer wheel enables the grinding process to appropriately grind free-form surfaces due to its capability to adapt to the grinding surface profile [28,29]. The significant benefit of a belt grinding process is attributed to the unnecessity of a coolant system as a grinding belt typically has a length of 2 to 5 m, which allows it for self-cooling [30].

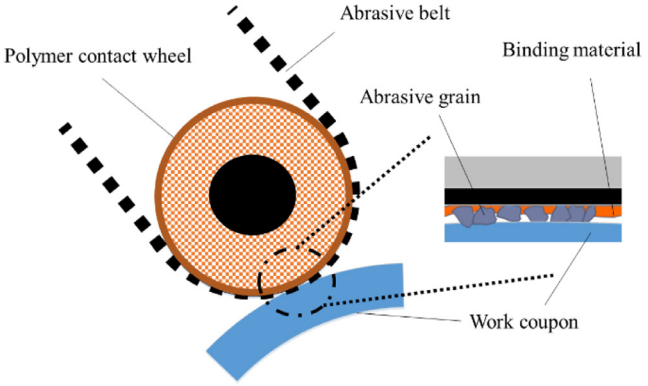

Fig. 1. The principle of belt grinding process.

The abrasive belt grinding process finds many exciting applications in various industries. Most commonly, it is used as a tertiary machining process to achieve desired stock removal and surface quality and to remove weld seam, burs or protruding features. The performance depends on the process parameters such as wheel speed, imparted force, abrasive grit size of the belt, feed rate, and polymer hardness. The cutting depth into the work coupon surface depends directly on the imparted force [31]. Belt grinding with contact wheels of different hardnesses changes the contact pressure in the interaction zone resulting in a change of wear mechanism. Material removal is also inversely proportional to the feed-in rate as the increase in dwell time of interaction between the grinding tool and workpiece surface results in higher stock removal [31]. Belt grinding parameter governs the rate of material removal by altering the contact conditions of the grinding wheel with the work coupon. The complex interaction between the workpiece and the abrasive belt results in a non-linear behaviour of the belt grinding tool.

2.2. VGG-16

VGG-16 is a convolutional neural network (CNN) architecture developed and refers to the Visual Geometry Group and is also called as OxfordNet. The VGG neural network is a CNN for classification of 1000 real-world objects. The VGG network helps to recognise objects based on output probabilities of the different classes that an image could potentially belong. VGG-16 takes an image of size $224 \times 244 \times 3$ as an input and deploys only 3×3 convolution and 2×2 pooling throughout the whole network architecture [32]. The schematic architecture of VGG-16 is illustrated in Fig. 2.

VGG has demonstrated that the depth of the network is beneficial for the classification accuracy and to give better results [32]. However, the major drawback of VGG-Net is that the network contains around 140 M parameters and most of the parameters are consumed in the fully connected layers [33]. To date, it is still considered to be an excellent pretrained vision model for solving classification problems, although it has been somewhat surpassed by more recent advanced networks such as Inception and ResNet [34].

2.3. Semantic segmentation

The primary goal of semantic segmentation is not only estimating the bounding box of the objects but also to assign each pixel present in an image to its corresponding class labels or none of them. Encoder-decoder based semantic segmentation helps in classifying and localising at the same time. Semantic segmentation is expressed as a discrete labelling problem that assigns each pixel $a_i \in \mathbb{R}^3$ of an image to a label b_i from a fixed set Z. Given N observations $a = [a_1, a_2, ..., a_N]$ the objective is to estimate the set of labels $b = [b_1, b_2, ..., b_N]$ taking the values in Z^N. It can be visualised as a supervised learning problem which requires

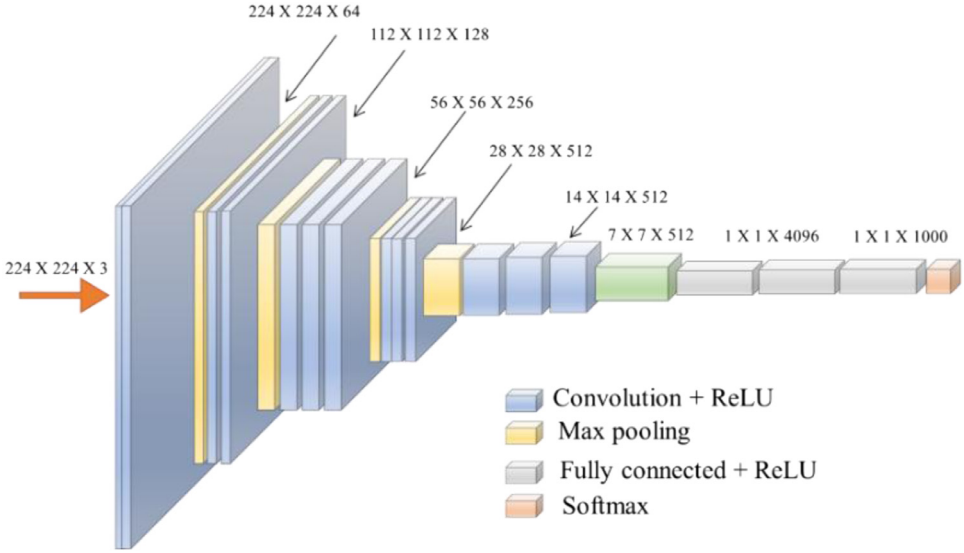

Fig. 2. The architecture of a VGG-16 network.

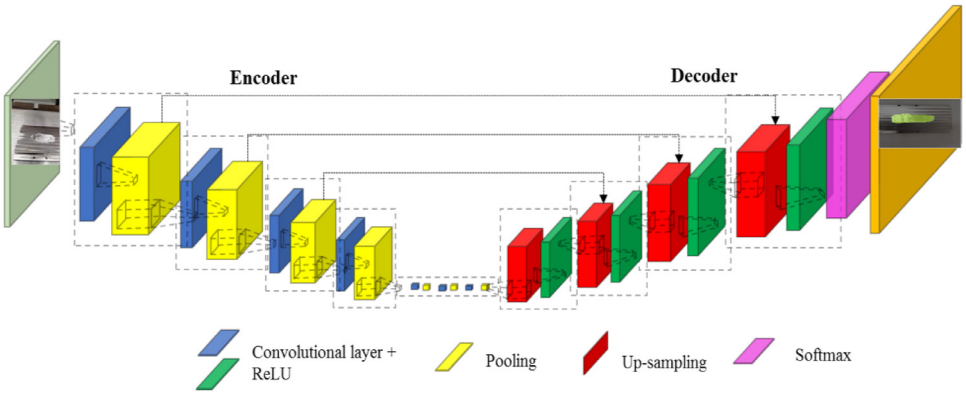

Fig. 3. An illustration of the encoder-decoder architecture.

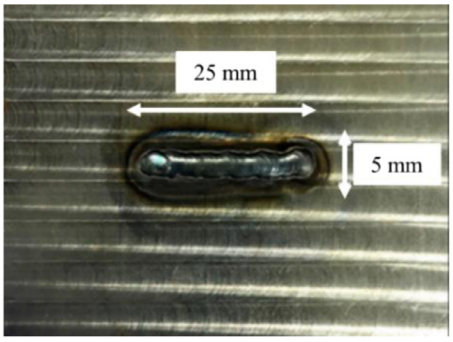

Fig. 4. Weld seam on the mild steel work coupon (top view).

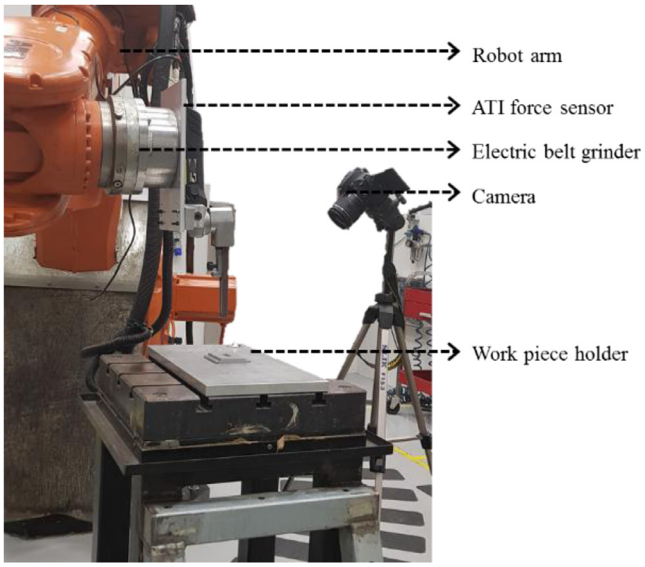

Fig. 5. Abrasive belt grinding setup with the camera.

training at the pixel level. Visual scene understanding in terms of geometry, depth, perception of shape can be achieved only using semantic segmentation architecture that has an encoder network followed by a decoder network which is a natural step in the progression from coarse to fine inference. A typical encoder-decoder architecture is illustrated in Fig. 3. The encoder is used to learn the discriminative deep features of the objects and the decoder is used to map the deep features of the objects on to a high resolutional image pixel space.

The primary task of the decoder is to semantically project the lower resolution discriminative features acquired by the encoder onto a higher resolution pixel space to get an intense classification. There are usually shortcut connections from the encoder to the decoder to help the decoder to recover the object details better and also to refine the upscaling process as shown in Fig. 3. The encoder performs a series of

Table 1
Parameters used in the belt grinding experimental trials.

Parameters	Description
Belt grinding speed	5000 ~ 11,000 RPM
Contact wheel diameter	10 mm, 24 mm
Hardness of contact wheel (polyurethane)	Shore A Hardness 30, 60, 90
Lubrication	Dry condition
Feed	10 mm ~ 40 mm
Belt finishing duration	Variable time
Operational mode	Position control

sequential convolutional operation on the images to learn the representation of multi-scale features. The layers are formed from shallow to deep convolutional layers. Shallow layers are likely to be formed with the dimensions equal to the original image input where the deep layers are formed with dimensions smaller than that of the original images. The decoder performs a series of convolutional transpose on the output of the encoder which increases the dimension of the deep feature maps to equal to the original image dimensions. The encoder is usually a pre-trained classification network like VGG/ ResNet/Alexnet etc. We adapt VGG-16 architecture as the encoder in this work.

3. Experimental setup and proposed methodology

3.1. Weld seam design and preparation

Weld seams are fabricated on a mild steel work coupon of dimension 80 mm × 75 mm × 10 mm with a consistent profile, and minimal spatter using Argon inert gas along with stainless steel (SUS308) filler rod as shown in Fig. 4.

Weld seams of consistent dimension 25 mm × 5 mm × 1.2 mm (L × B × H) are prepared and positioned at the center of all the work

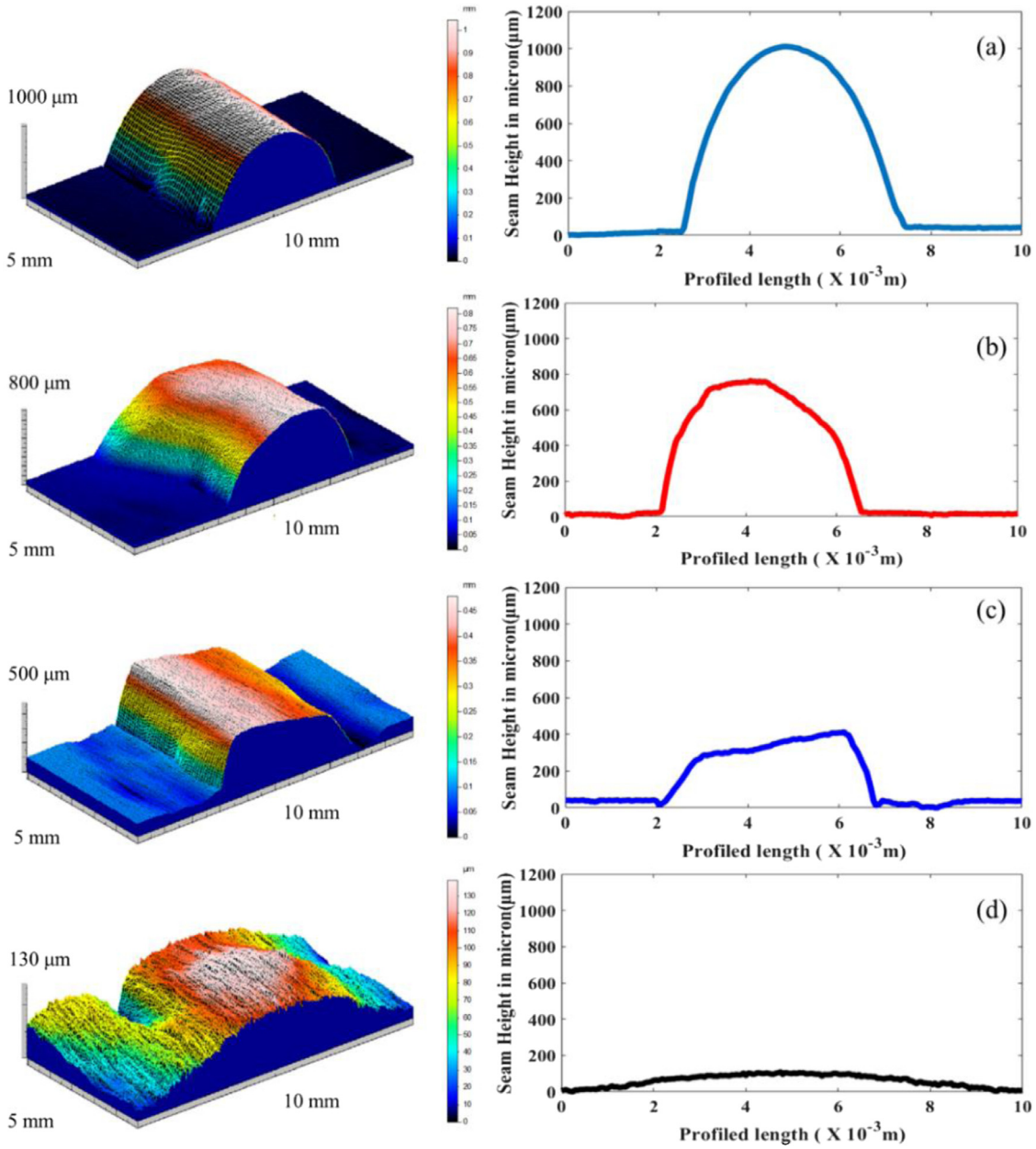

Fig. 6. (a) 3D and 2D profile extracted from across weld seam before belt grinding process (State-1); (b) 3D and 2D profile non-symmetrical profile extracted across the weld seam size when 30% is removed (State-2); (c) 3D and 2D profile non-symmetrical profile extracted across the weld seam size when 70% is removed (State-3). (d) 3D and 2D profile extracted when the weld seam is distinctively removed (State-4).

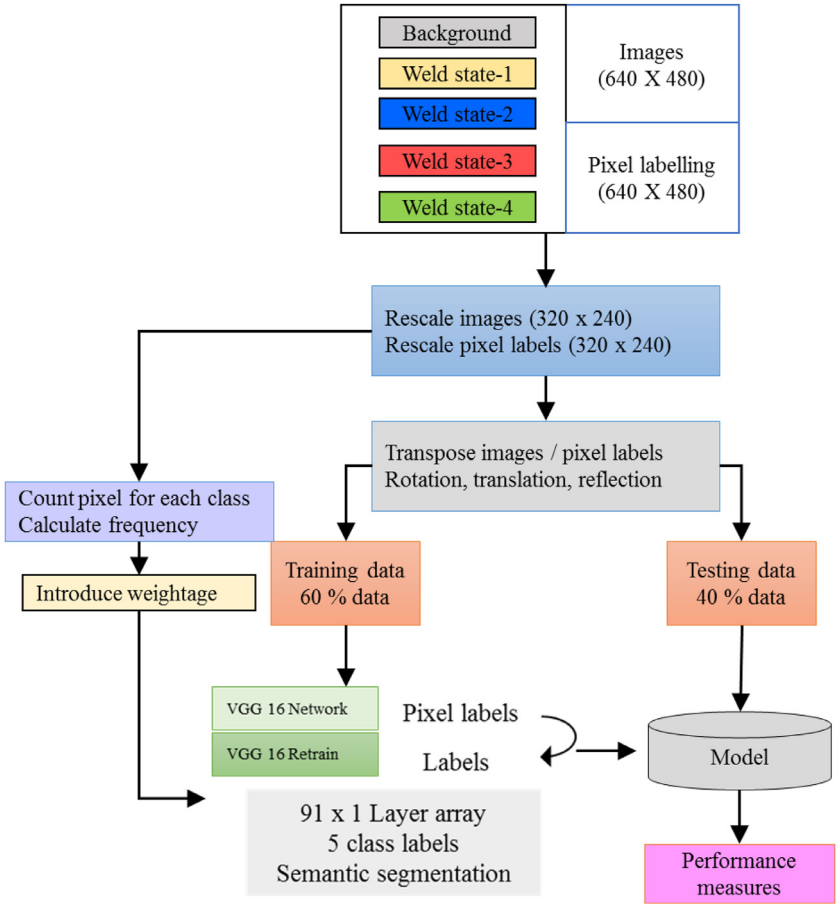

Fig. 7. General description of the proposed methodology.

Table 2
Weld state image datasets for training and testing.

Class	Type	Training sample	Testing sample	Colour map
Class 1	Background	1200	800	[000 000 000]
Class 2	Weld State-1	300	200	[192 200 20]
Class 3	Weld State-2	300	200	[000 000 192]
Class 4	Weld State-3	300	200	[192 000 000]
Class 5	Weld State-4	300	200	[128 192 000]

coupons used in the belt grinding trials. Robot-assisted grinding tool paths are prearranged to be perpendicular to the weld seam profile for the removal from the work coupon surface. In every pass of the tool on the weld seam, the weld seam profile height will be lessened. The robot will repetitively pass across the weld seam until the weld seam is completely removed.

3.2. Experimental setup and grinding conditions

Typically, an abrasive belt grinder consists of a couple of roller polymer wheels powered by an electric or pneumatic system and an abrasive belt. Fig. 5 shows the belt grinding setup used in the process. An abrasive belt supported by polymer wheels are run over a processed component at a certain speed to accomplish the grinding process. In our case, the polymer wheel is driven electrically.

The electrically powered tool motor used in our experimental trials is capable of running at 11,000 rpm at unloading condition and has the ability to driving the abrasive belt with the dimension of 3/4″ width 18″ length. This abrasive belt is made up of firmly coated silicon carbide grit with the size of 60. During the weld seam removal process, the belt wheel is kept normal to the surface of the workpiece to maintain a steady level of contact. The overall arrangement is fixed with a multi-axis robot (ABB 6660-205-193) on its end effector. The robot arm moves the grinder corresponding to the toolpath planned by the ABB Robot Studio software. Information about the grinding point is fed into the robot controller at every stage of grinding from which a closed-loop control was accomplished. The belt grinding parameter used during the weld seam removal are listed in Table 1. A vision system is introduced to capture the images of various stages of weld seam which consists of a digital camera and an image processing system. The digital camera is incorporated with the help of a tripod stand adjacent to the belt grinder as shown in Fig. 5. Surface images are captured at the end of every pass of robot arm across the weld seam. The camera system is capable of capturing and storing the surface images at a resolution of 1240 × 960 pixels which are subsequently fed into a pretrained algorithm to determine the endpoint.

3.3. Weld seam removal

Evolution of weld seam geometry during the removal process is labelled into four distinct classes based on the height of the weld seam geometry. Weld seam profiles are measured using Taly-scan profilometer, where the results are shown in Fig. 6 in the form of 3-Dimensional and 2-Dimensional profiles. As can be seen from Fig. 6(a), the shape of the weld seam profile before machining is symmetrical on both ends. This original state is, therefore, labelled as State-1. The weld profile appears hemispherical and symmetrical with its peak at the centre. The State-2 features an evolved weld profile as a result of grinding that is not symmetrical in shape with 30% of height removed compared to the weld profile obtained at the initial state as shown in

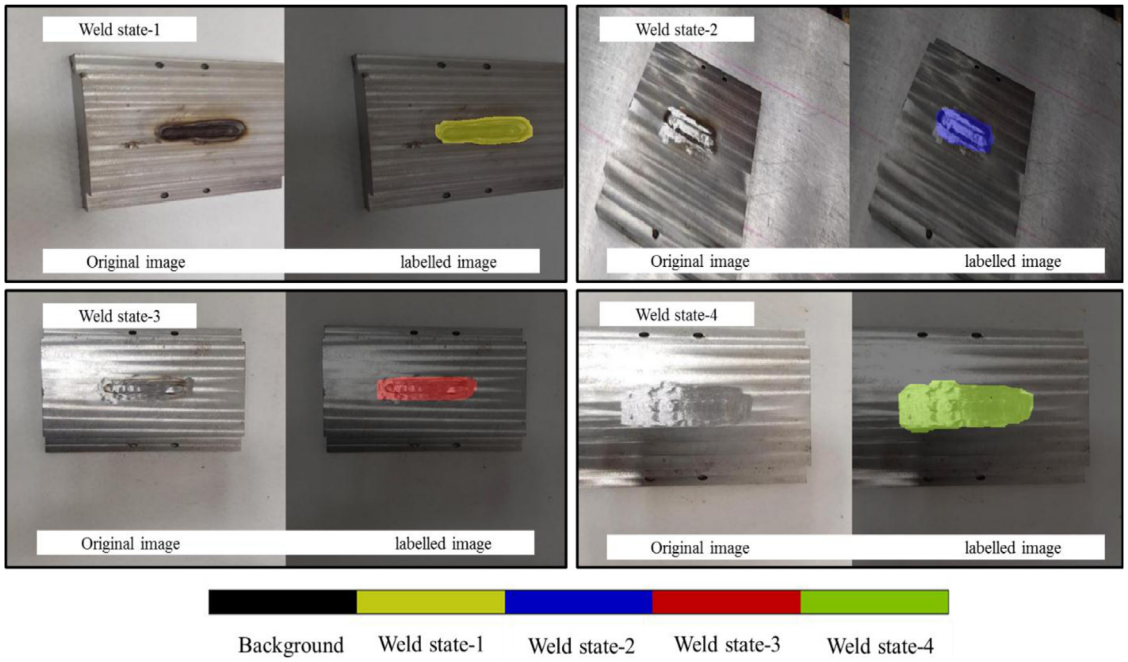

Fig. 8. Original and pixel labelled images of four different weld seam states.

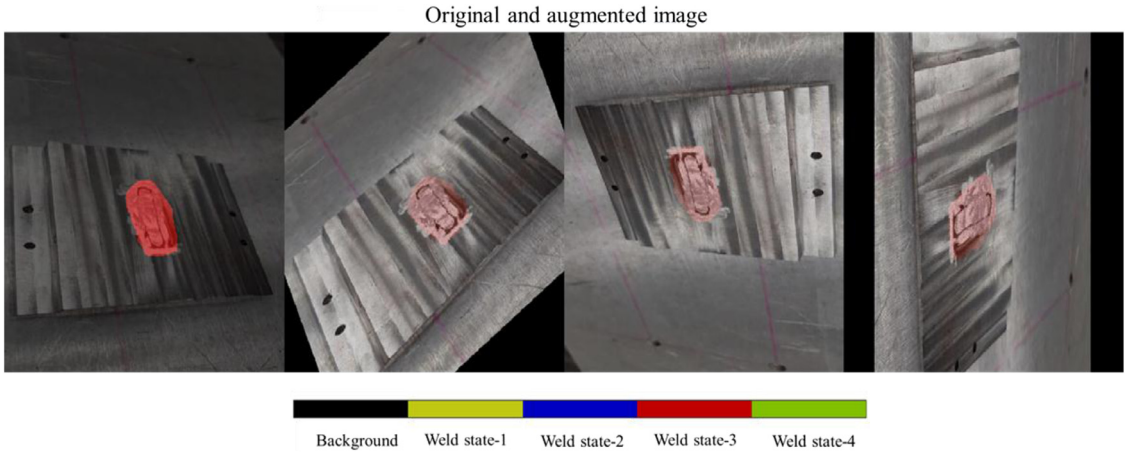

Fig. 9. Data augmentation on the work coupon with rotation and translation.

Fig. 6(b). The weld profile geometry of State-3 indicates the result of subsequent grinding which is not symmetrical in shape with 70% of height removed compared to the weld profile at State-1 as illustrated in Fig. 6(c). In State-4, the weld seam is distinctively removed as depicted in Fig. 6(d). This research tries to predict the State-4, i.e. the state of complete removal of weld seam from the work coupon, using a vision system and deep learning. We were able to visually confirm that only four distinct weld seam geometry profiles evolved during its removal process. Subsequently, we labelled each weld seam state into a classifier.

3.4. Methodology

Weld seam of four different removal states is machined with an abrasive belt with variable grinding conditions as listed in Table 1. Although the height of the weld seams cannot be accurately controlled, they were labelled as State-1, State-2, State-3 and State-4 based on their approximated height from initial height profile as 0%, 30%, 70% and 100%. The images at four different stages are taken in a consistent illumination, but with various angles, distances, rotations and motion blur. Each pixel of the images is labelled with its corresponding class, namely background, weld State-1, weld State-2, weld State-3, and weld State-4. Furthermore, the augmentations such as shear, random zoom, random crops are implemented to prevent overfitting and to involve randomness on the images. The augmented final image set is further split into two with 60% of the images for training and the remaining for testing. Training and testing images are split in such a way that they represent the probability distribution of all four possible weld seam state outcomes from the weld seam grinding process. The VGG-16 network is retrained to identify the weld seam states. Pixel labels layer of the default VGG-16 network is replaced by the customised labels layer that would identify the weld seam state and background of an image. Distribution of pixel count for four different belt states and background is identified, and the corresponding weight is redefined on the final layer of the VGG-16 network. The weld state identification was performed in MATLAB deep learning toolbox. The augmented training image set is used for training, and it is ensured that the training accuracy increases and training loss decreases with the iteration count. The training is terminated once the parametric conditions are met. The testing images are introduced into the retrained VGG-16 network, and

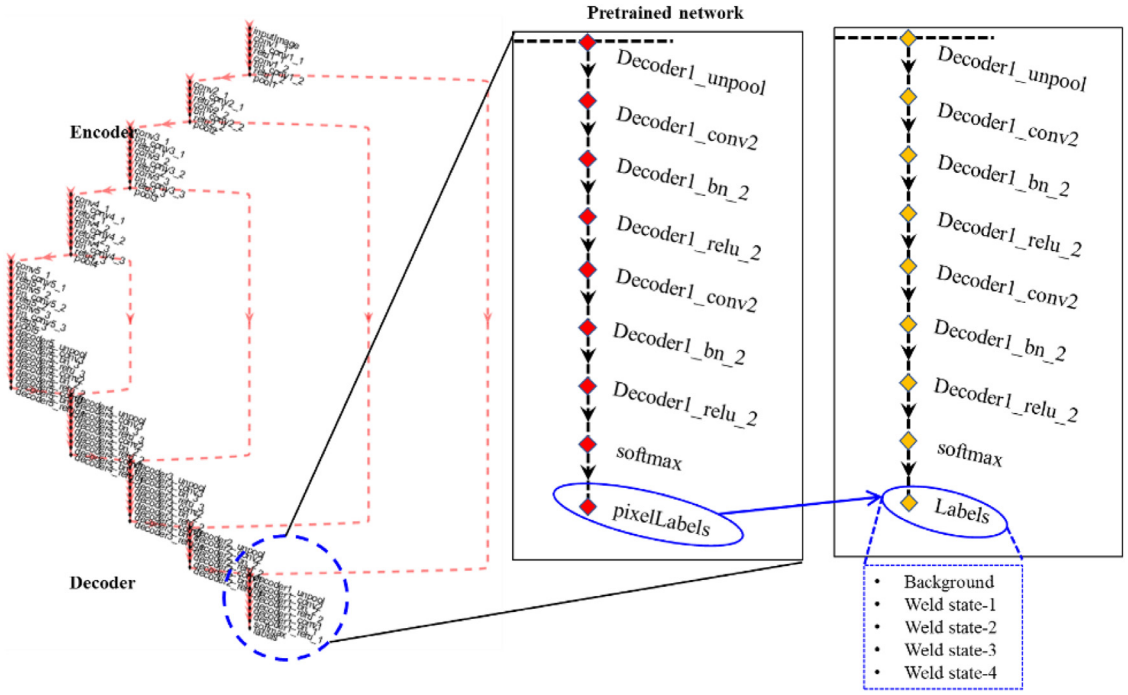

Fig. 10. Encoder-decoder architecture developed using VGG-16 to predict the weld seam states.

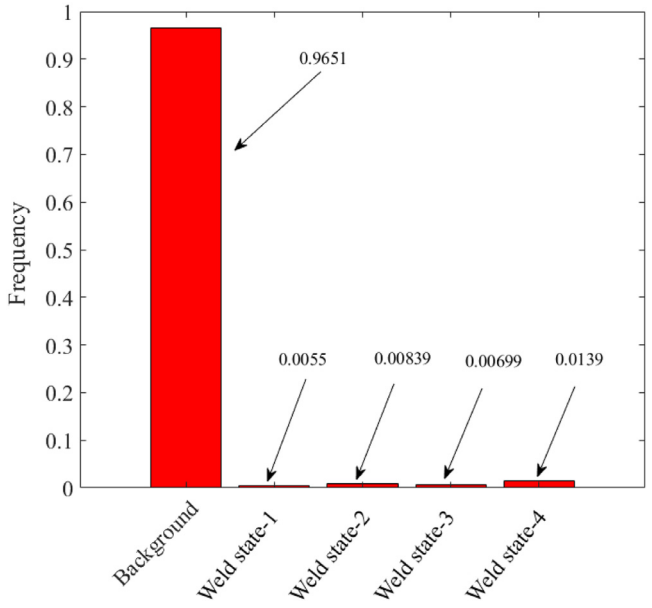

Fig. 11. Distribution of pixels for four different belt states and background.

the network prediction and ground truth label values of the images are equated to identify the network performance. Schematic representation of the methodology is described in Fig. 7.

4. Endpoint detection of weld seam removal

4.1. Image acquisition and data preparation

A vision system consisting of a DSLR Nikon camera is introduced to capture the images of various states of the weld seam. The digital camera is placed adjacent to the robot arm such that its field of view is not interrupted by robots end effector and belt grinder assembly. Weld seam images at the four different states are captured at the end of every pass of belt grinder across the mild steel work coupon. The weld seam images representing four different states are taken in such a way that they contain a broad range of image distribution pattern. Please note, as indicated before, images are taken in constant illumination, but the angle, distance, rotation, and orientation are varied.

Table 3
SegNet training parameters.

Segmentation training parameters	Values
Type of analysis	Semantic segmentation
Solver name	'sgdm'
InitialLearnRate	0.001
L2Regularization	0.0005
MaxEpochs	30
MiniBatchSize	5
LearnRateSchedule	piecewise
LearnRateDropFactor	0.2
LearnRateDropPeriod	5
Shuffle	Every-epoch
Training set	60%
Testing set	40%

Each pixel is labelled using colourmap as listed in Table 2 based on the weld seam state and background. Fig. 8 illustrates the semantic pixel-wise labelling, i.e., labelling each pixel of an image for four different weld seam states with ground truth label using the colourmap. The ground truth labels with the corresponding colour map are implemented using the image labeller available within the MATLAB framework.

Data augmentation provides the possibilities of increasing the input image distribution and it also helps in the generalisation of the network. Data augmentation is a technique to artificially increase the training set by adding transformations or perturbations of the training data without increasing the computational cost. Fig. 9 shows how augmentations such as rotations, horizontally or vertically flipping and random crops are implemented in the images. The augmented final image set is further split into two with 60% of the images for training the network and the remaining for testing as listed in Table 2. In total, 2000 images taken using the DSLR vision system are used for this study out of which 1200 images are used for training the network and remaining 800

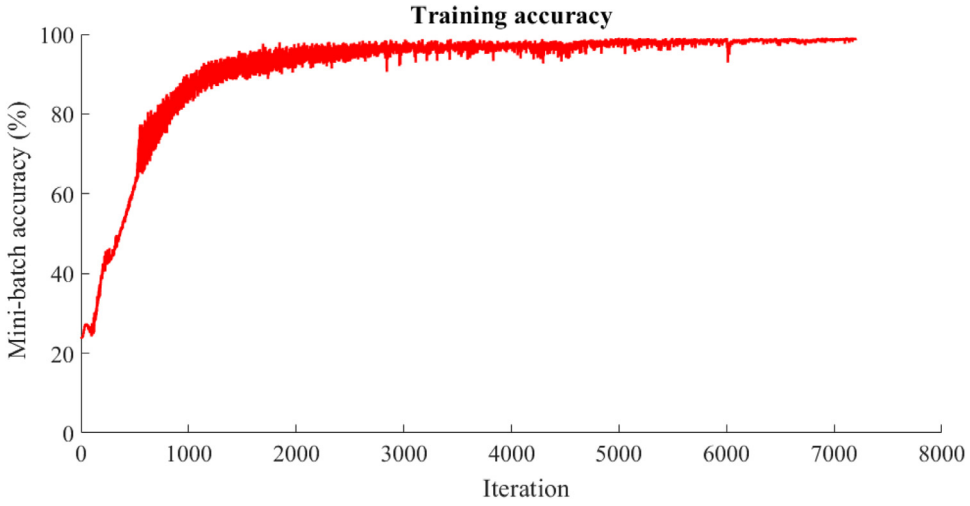

Fig. 12. Training accuracy during retraining VGG-16 network for weld seam state prediction.

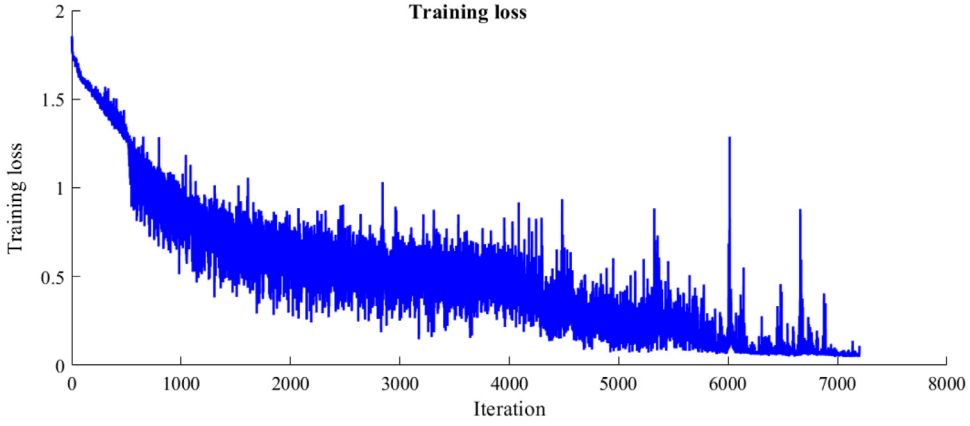

Fig. 13. Training loss during retraining VGG-16 network for weld seam state prediction.

Table 4
High-level overview of the network performance.

Class	Accuracy	IoU
Background	0.98838	0.98821
Weld State-1	0.99855	0.73091
Weld State-2	0.98398	0.75043
Weld State-3	0.99801	0.71128
Weld State-4	0.99858	0.78358

Table 5
Weld seam state detection results in using SegNet.

Parameter	Value
Mean accuracy	0.9935
MeanIoU	0.79288
WeightedIoU	0.98006
Global accuracy	0.98861

images are implemented for testing purpose. These training and testing images are considered to be the representation of the probability distribution of the possible four weld state outcomes from the grinding process. The same distribution of images is strictly considered for the training and testing of the network. The training of the network is carried out in an offline process. From the large pool of the training data, each class has 500 instances or images as listed in Table 2.

4.2. Development of the VGG-16 framework

Implementation of a sophisticated image recognition models requires tuning of millions of parameters. Building and training such a model from scratch requires a lot of computing power and a lot of labelled training dataset. However, a VGG-16 model architecture that has already been familiar with a related task is taken and reused. An encoder-decoder architecture is built using the pretrained VGG-16 network to perform image segmentation by assigning each pixel in an image to the corresponding class. The encoder-decoder network consists of 91 layers including convolution, batch normalization, pooling, unpooling and the pixel classification output layers. As shown in Fig. 10 the image is first down sampled by an encoder part as in a VGG-16 pretrained model, and then it is up sampled by using a decoder part that more-or-less looks like a reversed VGG-16 architecture. Encoder-decoder architecture developed using the VGG-16 network is modified by replacing a couple of layers as shown in Fig. 10 to suit the weld seam state recognition problem statement. The classes in weld seam data set are imbalanced as shown in Fig. 11 as all classes did not have an equal number of pixel count. The background class covers a larger area and pixel count value compared to the other weld seam state which makes the learning biased more towards the dominant background class. To improve training and remove the biasing towards the dominant class the weight of the classes are balanced using median frequency. The weights of the weaker classes are given higher value and vice versa based on the median frequency score in pixelClassificationLayer.

We use MATLAB to convert the collected datasets to the SegNet data

	Background	Weld state-1	Weld state-2	Weld state-3	Weld state-4
Background	100%	27%	24%	29%	22%
Weld state-1	0%	73%	0%	0%	0%
Weld state-2	0%	0%	76%	0%	0%
Weld state-3	0%	0%	0%	71%	0%
Weld state-4	0%	0%	0%	0%	78%

Fig. 14. Confusion matrix on the pixel-wise classification of weld seam state prediction.

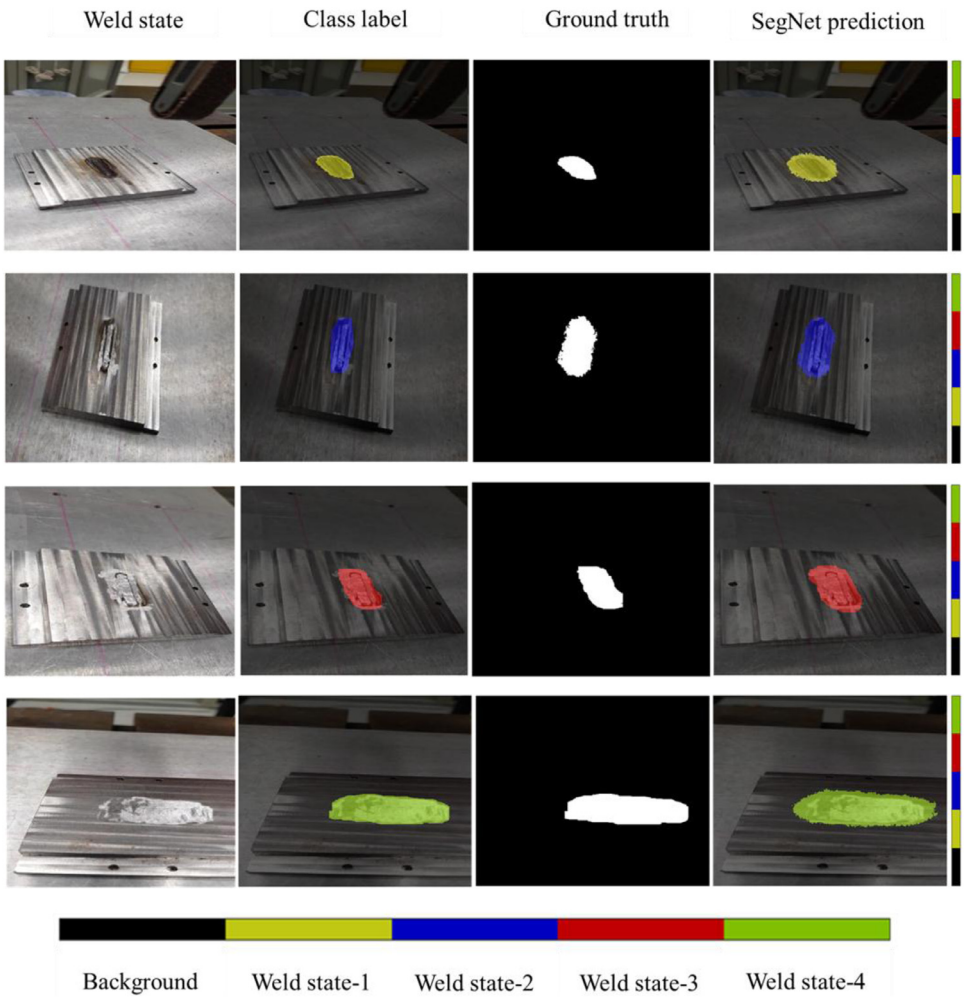

Fig. 15. Qualitative assessment of SegNet predictions on weld seam states using modified VGG-16 architecture.

format and annotate the images. For model training, we use NVIDIA®GeForce®GTX10870 module on a desktop computer. The optimisation algorithm used for training is stochastic gradient descent with momentum. A minibatch size of five is used to reduce memory usage while training. For model training, the parameters listed in Table 3 are used. The average model training time in reaching a maximum number of iterations of 7200 is 8 hrs.

Two different metrics such as training accuracy and training loss are used to evaluate the performance of the deep learning model during its training phase. Training loss is often used in the training process to find the best parameter values for model considered to minimize the error and training accuracy is more on the ability of the model prediction compared to the true data. The primary objective of training a deep learning model is to reduce the loss function's value with respect to successive iteration count. Fig. 12 shows the plot of model accuracy and Fig. 13 shows the plot of model loss during model training. Upon visualising training accuracy and training loss plots, it is evident that there exists inverse proportionality relationship which confirms training progress is successful. From the plot of accuracy, we can see that the model has been thoroughly trained as the trend for accuracy

training datasets saturates at 4000 iterations and there is subtle performance improvement beyond this.

4.3. Result and discussion

The performance of the trained architecture is determined by the good prediction made over the true events. Eight hundred images are considered for testing of the trained architecture. By comparing the predictions made by the architecture over the labelled subset in testing data, the performance of the architecture can be determined as shown in Tables 4 and 5. Intersection over union (IoU), which is the measure of the area of overlap and area of the union, is used as an evaluation metric to measure the accuracy of the trained architecture on a testing dataset. The individual IoU of each class, meanIoU scores and weightedIoU scores from Tables 4 and 5 suggest satisfactory predictions results.

The absorbed true positive, true negative, false positive, false negative of the modified VGG-16 SegNet model on each pixel of the test data set are given in Fig. 14. The figure shows that there is no misclassification among the four weld seam states. However, there is a noticeable misclassification between the background class and four weld seam states. This mostly occurs when weights are not optimized in the pixel classification layer of the network. Even though we had taken into account the bias and tendency of the network towards the dominant background using median frequency, the weights still can be further tuned to differentiate between the weld seam states and background.

Fig. 15 shows the qualitative evaluation of the performance of the model. In the figure, we present four instances of all weld state data, default colour coded pixel-wise labels, ground-truth, and network prediction output for visual inspection. The first column shows the input image followed by colour-coded labels and ground truth label in column two and three followed by network output in column 4 with corresponding colour codes in each pixel of the image.

5. Conclusion

We have demonstrated a novel method for weld seam removal detection based on images taken using a DSLR camera using CNN-based semantic segmentation. The encoder-decoder based modified VGG-16 architecture is trained on images obtained from an actual belt grinding process on mild steel work coupon for weld seam removal. The proposed method achieves a competitive segmentation precision on the testing dataset. The prediction system based on semantic segmentation is able to identify weld profile geometry evolution irrespective of the variable grinding parameters. This approach will allow us to optimize the process further. The proposed methodology is also capable of removing weld seams from free-form surfaces on further optimization of tool path planning and image acquisition.

Although it results in a high classification accuracy of the weld seam states, misclassification between weld seam states and background was also found higher. The high classification error between the weld seam states and the background is attributed to the fact that background class covers larger area and pixel count value compared to those of the weld seam state. In the future, we intend to improve the performance of the proposed network and reduce the misclassification between weld seam states and background by localising the work coupon from the background and feed the region of interest (ROI) into the encoder-decoder network to narrow down the search region. It is expected that it will offer a much faster and efficient architecture to facilitate a real-time decision in predicting the endpoint of weld seam removal.

As a final words, we have presented our work based on VGG-16 network and implementation of the method on other pretrained models are still in progress. Augmenting the robot further with vision-guided machining mechanism in locating and localizing the work coupon and weld seam will further optimize the process which will be a future work.

Acknowledgement

This work was conducted within the Rolls-Royce@NTU Corporate Lab with support from the National Research Foundation (NRF) (Grant No. M-RT1.1 M4061298) Singapore under the Corp Lab@University Scheme.

References

[1] S. Kurada, C. Bradley, A review of machine vision sensors for tool condition monitoring, Comput. Ind. 34 (1) (1997) 55–72 1997/10/01/.
[2] M.U. Islam, L. Xue, and G. McGregor, "Process for manufacturing or repairing turbine engine or compressor components," Patent U.S. Patent 6269,540., 2001.
[3] P.W. Heitman, S.N. Hammond, and L.E. Brown, "Method for joining single crystal turbine blade halves," Patent U.S. Patent 5071,059., 1991.
[4] D. Axinte, M. Kritmanorot, M. Axinte, N. Gindy, Investigations on belt polishing of heat-resistant titanium alloys, J. Mater. Process. Technol. 166 (3) (2005) 398–404.
[5] V. Pandiyan, T. Tjahjowidodo, In-process endpoint detection of weld seam removal in robotic abrasive belt grinding process, Int. J. Adv. Manuf. Technol. 93 (November (5)) (2017) 1699–1714.
[6] X. Xu, D. Zhu, J. Wang, S. Yan, H. Ding, Calibration and accuracy analysis of robotic belt grinding system using the ruby probe and criteria sphere, Rob. Comput. Integr. Manuf. 51 (2018) 189–201.
[7] H. Xie, C.T. Pang, W.-L. Li, Y.-H. Li, Z.-P. Yin, Hand-eye calibration and its accuracy analysis in robotic grinding, 2015 IEEE International Conference on Automation Science and Engineering (CASE), 2015, pp. 862–867.
[8] W.-L. Li, H. Xie, G. Zhang, S.-J. Yan, Z.-P. Yin, Hand-eye calibration in visually-guided robot grinding, IEEE Trans. Cybern. 46 (11) (2016) 2634–2642.
[9] X. Ren, M. Cabaravdic, X. Zhang, B. Kuhlenkötter, A local process model for simulation of robotic belt grinding, Int. J. Mach. Tools Manuf. 47 (6) (2007) 962–970.
[10] J. Kojima, Weld Bead Removing Apparatus, in: Google Patents (Ed.), 1974.
[11] D.E. Whitney, A.C. Edsall, A.B. Todtenkopf, T.R. Kurfess, A.R. Tate, Development and control of an automated robotic weld bead grinding system, J. Dyn. Syst. Meas. Contr. 112 (2) (1990) 166–176.
[12] Y. Ito, In-process measurement for machining states: sensing technology in noisy space, Thought-Evoking Approaches in Engineering Problems, Springer, 2014, pp. 17–40.
[13] J.C. Chen, L. Huang, A. Lan, S. Lee, Analysis of an effective sensing location for an in-process surface recognition system in turning operations, J. Ind. Technol. 15 (3) (1999) 1–6.
[14] R.C. Luo, M.G. Kay, A tutorial on multisensor integration and fusion, Industrial Electronics Society, 1990. IECON'90., 16th Annual Conference of IEEE, IEEE, 1990, pp. 707–722.
[15] D. Dornfeld, Acoustic emission process monitoring for untended manufacturing, Proc. Japan-USA Symposium on Flexible Automation, 1986, pp. 831–836.
[16] X. Chen, S. Chen, T. Lin, Y. Lei, Practical method to locate the initial weld position using visual technology, Int. J. Adv. Manuf. Technol. 30 (7) (2006) 663–668 2006.
[17] H. Luo, X. Chen, Laser visual sensing for seam tracking in robotic arc welding of titanium alloys, Int. J. Adv. Manuf. Technol. 26 (9) (2005) 1012–1017 2005.
[18] T. Mikolajczyk, Indication of machining area with the robot's camera using, Appl. Mech. Mater. 282 (2013) 146–151.
[19] G. Sutter, L. Faure, A. Molinari, N. Ranc, V. Pina, An experimental technique for the measurement of temperature fields for the orthogonal cutting in high speed machining, Int. J. Mach. Tools Manuf. 43 (7) (2003/2003) 671–678 05/01/.
[20] Y. LeCun, Y. Bengio, G. Hinton, Deep learning, Nature 521 (2015) 436 05/27/online.
[21] N. Audebert, B. Le Saux, S. Lefèvre, Segment-before-detect: vehicle detection and classification through semantic segmentation of aerial images, Remote Sens. 9 (4) (2017).
[22] R. Yasrab, N. Gu, X. Zhang, An encoder-decoder based Convolution Neural Network (CNN) for future Advanced Driver Assistance System (ADAS), Appl. Sci. 7 (4) (2017).
[23] E. Chong, C. Han, F.C. Park, Deep learning networks for stock market analysis and prediction: methodology, data representations, and case studies, Expert Syst. Appl. 83 (2017/2017) 187–205 10/15/.
[24] M. Sheinfeld, S. Levinson, I. Orion, Highly accurate prediction of specific activity using deep learning, Appl. Radiat. Isot. 130 (2017/2017) 115–120 12/01/.
[25] I. Sa, et al., weedNet: dense semantic weed classification using multispectral images and MAV for smart farming, IEEE Rob. Autom. Lett. 3 (1) (2018) 588–595.
[26] G. Serin, M.U. Gudelek, A.M. Ozbayoglu, H.O. Unver, Estimation of parameters for the free-form machining with deep neural network, 2017 IEEE International Conference on Big Data (Big Data), 2017, pp. 2102–2111.
[27] V. Badrinarayanan, A. Kendall, R. Cipolla, SegNet: a deep convolutional encoder-decoder architecture for image segmentation, IEEE Trans. Pattern Anal. Mach. Intell. 39 (12) (2017) 2481–2495.
[28] X. Zhang, B. Kuhlenkötter, K. Kneupner, An efficient method for solving the Signorini problem in the simulation of free-form surfaces produced by belt grinding, Int. J. Mach. Tools Manuf. 45 (6) (2005) 641–648.
[29] A. Khellouki, J. Rech, H. Zahouani, The effect of abrasive grain's wear and contact

conditions on surface texture in belt finishing, Wear 263 (1) (2007) 81–87.
[30] H. Tschätsch, A. Reichelt, Abrasive belt grinding, in: H. Tschätsch (Ed.), Applied Machining Technology, Springer Berlin Heidelberg, Berlin, Heidelberg, 2009, pp. 297–299.
[31] H. Huang, Z. Gong, X. Chen, L. Zhou, Robotic grinding and polishing for turbine-vane overhaul, J. Mater. Process. Technol. 127 (2) (2002) 140–145.
[32] K. Simonyan, A. Zisserman, Very Deep Convolutional Networks for Large-Scale Image Recognition, (2015).
[33] M.G. Ertosun, D.L. Rubin, Probabilistic visual search for masses within mammography images using deep learning, 2015 IEEE International Conference on Bioinformatics and Biomedicine (BIBM), 2015, pp. 1310–1315.
[34] A. Canziani, A. Paszke, E. Culurciello, J. CoRR, An Analysis of Deep Neural Network Models for Practical Applications, (2016) vol. abs/1605.07678.